ICAS-84-1.2.2

Analysis of Transonic and Supersonic Flows around Wing-Body-Combinations

Stefan Leicher
Dornier GmbH, Friedrichshafen, West Germany

Abstract:

The Dornier full potential and Euler methods in combination with a general mesh generation code are used to calculate trans- and supersonic flows around wings, wing-body combinations and bluff bodies. A short description of the two flow solvers and of the grid generation program will be given. More detailed information is included in the comparison between our Euler method in blocked and unblocked form and the very recent combination of both forms with a multigrid technique. Results will be shown for wings, wing-body combinations, flows with embedded vortices and flows around a bluff body such as a car.

Introduction

Successful computational algorithms for the transonic full potential equation and the Euler equations have been evolved to solve three-dimensional problems [1-4]. A very efficient algorithm is the finite volume approach for both the full potential as well as for the Euler equations, because the boundary conditions can be easily implemented. Furthermore, the finite volume methods combined with contour conformal meshes allow the treatment of complex geometries and are, in connection with block-structure grids and flow solvers, applicable to nearly all three dimensional flow problems.

Mesh Generation

The contour conformal meshes used for both the full potential as well as for the Euler methods are generated by solving a set of suitable chosen partial differential equations [5,7]. Depending on the complexity of the problem, either a Single-Block (SBG) [6,7] or a Multi-Block (MBG) grid is used [7,8]. In both cases the same equations are solved. In the case of the SBG this is done for the whole grid domain at once. According to the complex geometry the MBG methods divides the whole mesh in several well chosen sub domains, which can be defined arbitrarily to produce surface fitted grids that follow the natural lines of the configuration. In both cases, the surfaces of the configuration and a one-dimensional perimeter discretization along the block perimeters has to be established first. This provides boundary conditions for a subsequent two-dimensional grid generation, producing grids covering the block surfaces, body parts excluded. Once having resolved all surfaces, the 3-D grid interior is obtained by solving a set of Poisson equations of the form

$$\vec{U}_{xx} + \vec{U}_{yy} + \vec{U}_{zz} = \vec{P}\ (u,v,w)$$

with the computational coordinates $\vec{U} = (u,v,w)$ and the source terms $\vec{P} = (P,Q,R)$ to control the interior grid spacings [5]. Some examples of grids constructed in this manner will be shown below, in the discussion of the results.

Flow Methods

The Dornier FPE method is a full conservative finite volume method with a SLOR-scheme that was only applicable to SBG-type meshes until now. In the last years very fast iteration procedures for solving the 3-D full potential equation, such as ADI [9,10] or multigrid techniques [11,12] have been developed. This makes these methods still attractive today, although they are not exactly correct when shocks occur in the flow field. Combined with a threedimensional integral boundary layer method [13], our method is able to account for viscous effects.

The Euler equations give an exact description of inviscid transonic flow. Our time dependent finite volume Euler method uses a three or four stage Runge Kutta scheme [14], which turns out to give, combined with a multi level grid technique, very fast convergence even for very fine meshes. Because the Euler methods require more variables to be stored, in core a mesh size of about 97x17x17 is the maximum possible using a 1 million word computer. For this reason we developed a Multi Block Version (MBV) of our code, which divides the flow field into a number of blocks and the flow variables are stored on disk files. Since this procedure allows each block to be solved separately, the overall mesh size can be increased to a grid size giving realistic resolution for 3-D flow problems. One restriction for blocked codes is the rate between I/O- and CPU-time. We have spent a lot of work on this problem, rewriting our code while interchanging the block- and Runge Kutta loop, using asynchronous Read- and Write statements and using special file distribution on special disk devices. One further step was the development of a so-called Dynamically Blocked Version (DBV). While the Fixed Blocked Version (FBV) keeps the block structure constant through all meshes of a multi-level grid technique, the DBV-code is able to change this structure during computation. The DBV-version really keeps the subgrids unblocked with all variables in core, up to the finest grid where blocking really is only necessary. The actual dimensions of the maximum unblocked grid depends therefore on the storage which is available. The dimensions can be easily changed by input. With all these improvements the rate between I/O and CPU time could be kept between .2, for a normal three level grid technique using the DBV, and .3, for the FBV using 18 blocks.

Very recently convergence and computing time of the code has been further improved by using a multigrid scheme like that proposed by Jameson [15]. This multigrid technique has already been combined with our FBV as well as our DBV-Euler

codes. First results and comparisons of the convergence behaviour for unblocked-, blocked single-grid and unblocked- and blocked-multigrid calculations in terms of the averaged $d\rho/dt$, and the number of supersonic points or the drag coefficient are given in the figures 1.-3..

The well-known ONERA M6 Wing has been chosen to demonstrate the efficiency of the new Euler Multigrid Fixed Blocked (EMG FBV) and Dynamically Blocked (EMG DBV) version of our Euler code. Compared are blocked results with and without and unblocked with and without using the multigrid technique. The mesh size was 97x17x17. These dimensions allow a maximum of 3 multigrid levels, even when the mesh is blocked once in one or more directions. Figure 1a. compares the averaged $d\rho/dt$ reduction for a 4 and 3 stage Runge Kutta scheme for the unblocked case with and without using the multigrid technique. Obvious is the improvement of the multigrid scheme, where the 3 stage scheme seems to be the more efficient one. Figure 1b. shows quite clearly that the result using multigrid needs only about 100 time steps to reach a converged solution. Figure 2. compares unblocked and blocked results with and without multigrid. Figure 2a. shows the error reduction and development of the supersonic zone for different block numbers using multigrid, while figure 2b. shows the same comparison without multigrid. With larger block-numbers the waviness of the curves seems to increase. For the normal scheme the overall convergence is nearly the same, while for the multigrid cases the reduction as well as the final error level seems to increase with the number of blocks. The increase after about 150 time steps for all multigrid cases has been observed previously and is caused by a nonoptimal solution scheme. As figure 2c. and d shows, this can be corrected with a 3 stage scheme using well chosen coefficients and filter terms. Nevertheless figure 2a. shows that the final solution is reached after about 100 cycles; without multigrid 500 cycles seem still too few, as the non-zero slopes at the end of the curves indicate. Unfortunately for the 4-block case one block boundary hits exactly the wing tip section. This may be an explanation for the greater differences in the error plots as well as for the loss of supersonic points compared with the two other cases. The block boundaries have to be choosen quite carefully. Also for the blocked multigrid cases the flow values and intermediate properties at the boundaries are not transferred from one block to the neighbouring one but are interpolated from the higher level values to minimize the I/O-work. If one omits this, a further acceleration may be possible.

Figure 3. shows results from our FBV-Euler code for a case with a rather coarse grid around an ellipsoid. For test purposes these calculations were carried out in a total mesh of 33x17x17 points, being divided into 18 blocks. Therefore the minimum blocksize was 17x5x5, allowing only 2 multigrid levels. Compared are the 3 stage Runge Kutta scheme with and without multigrid and the 4 stage scheme without multigrid technique. Both the convergence behaviour (Figure 3a.) and the development of the drag (Figure 3b.) shows the great advantage of the new multigrid method. Although only 2 multigrid levels and such an extremely high block-number were used, the final results were achieved in less than 100 time steps. Again the 3-stage scheme turns out to be the more efficient one. Figure 3c. shows the calculated pressure distribution compared with the analytical solution. The agreement for such a coarse grid is rather good, although some problems seem to rise at the block boundaries.

Results

Results for both the full potential and the Euler methods compared with other methods and experiments will be shown below. The first example shows differences between Euler and FPE computations using the same grid. The second example shows that in some cases it is necessary to perform "real body" calculations to get realistic answers. The last examples show Euler results with embedded vortices, such as leading edge vortex flow and vortices emanating from sharp corners.

Transport type aircraft

For a transport type aircraft the differences between FPE and Euler method are shown in the figures 5. to 7., while figure 4. shows the body and wing surface grid for a total mesh size of 161x33x33. The calculations were actually performed in a mesh being half as large.

The pressure distributions in figure 5. show quite clearly some differences. According to the total pressure loss across the strong shock, which can be accounted for only by the Euler method, we obtained different stream angles at the trailing edge for both methods, resulting in a different trailing edge pressure. This is comparable with a different angle of attack and of course affects the whole pressure distribution on the lower as well as on the upper surface. The Euler method also seems to resolve a sharper shock, while using the same grid. The load distribution in the spanwise direction reflects these pressure differences as shown in figure 6. Lastly, figure 7. shows the comparison of the center line pressure of the body calculated by the FPE and experimental data.

Fighter type aircraft

For a fighter aircraft, whose surface grid can be seen in figure 8., many computations have been performed. Figure 9a. shows the results for two calculations with infinite cylindrical bodies compared to a wing alone case. In the case of the small fuselage it resulted in a similar displacement effect and in the case of the large body it was attempted to simulate the real channel geometry between the lower side of the wing and the engine cowl. The computed differences are rather small and especially the cp-values in the region of the channel still show great differences with the measurements.

The inclusion of the real body shape as shown in figure 9b. improved the theoretical results greatly. The lower side pressure distribution now shows good agreement with the data and the upper side values have also improved. Quite obvious are the differences between the wing alone and the "real body" results.

Flows with vortices

As in [16], the time-dependent Euler methods are able to produce flows with embedded vorticies, although they do not account for viscous effects. There are two explanations for this. First, according to Croco, vorticity is produced by entropy changes like those occurring across a shock with variable strength. If such a curved shock is detected some time during the iteration cycle, the produced vorticity will be conserved even though the steady state solution shows no supersonic region at all. The second explanation is that the numerical scheme itself produces a numerical viscosity which also introduces vorticity. Both mixed together enables the Euler methods to calculate cases with embedded vorticies, forced by flows around sharp corners, where very high mach numbers even at low subsonic free stream conditions can be encountered.

One well-known phenomena in aircraft aerodynamics is the so-called leading edge vortex of slender wings with sharp leading edges even at relatively low angles of attack. This vortex consists of a free shear layer, which emerges from the leading edge and rolls up above the wing forming one concentrated vortex.

Figure 10. shows the representation of the Boeing Arrow wing configuration in our 3-D calculation. This configuration was tested for a wide range of different flow conditions. The results for one subsonic case is given in figure 11.-14.. Figure 11. shows the wing pressure distribution with the maximum negative cp just below the vortex axis. Figure 12. gives a comparison between calculated and measured pressure values at several cross-flow planes. This figure as well as figure 13., which compares the lift coefficients shows good agreement with measurements. The curve between $\alpha = 16^{\circ}$ and $\alpha = 35^{\circ}$ is not a computed one, but we know from other theories that this point lies in the region of vortex breakdown. Even flow details, such as the trailing edge vortex [17] and the behaviour of the total pressure loss [18], which are compared in [19], seem to be predicted quite well. Figure 14a.,b. shows the velocity distribution and the corresponding vorticity field at several cross-flow planes.

Another example for leading edge vortex flow is the Dillner delta wing. Figure 15. shows the wing surface grid with about 3000 points on the contour, while using a total number of about 200,000 points. All results shown below are computed in a mesh being twice as large with about 4000 points on the surface. This calculation was done in an AGARD working group for 3-D Euler methods.

Figure 16. shows the comparison between computation and experiment for $M_{\infty} = .7$, $\alpha = 15^{\circ}$ and figure 17. for $M_{\infty} = 1.5$, $\alpha = 15^{\circ}$. Figure 18. shows the calculated velocity field compared with experimental data. In all figures the agreement is quite good. Unfortunately no other experimental data for comparison is available for this wing. Flow measurements for such interesting cases are rather seldom.

That a vortex can not only be caused by a sharp leading edge may be shown by the next example, a stand-off missile with a rectangular body section having relatively sharp corners (Figure 19.). Analysing the final result of the calculated lift coefficients for three mach numbers and two angles of incidence (Figure 20.) we found good agreement between the Euler results and the experimental data for the lower angle, while for the higher one it is still satisfactory. Also plotted are results for a panel method, which shows great differences at $\alpha = 6^{\circ}$ and an unacceptable discrepancy at $\alpha = 12^{\circ}$. Figure 21a. shows schematically where these differences come from. The flow around the sharp corner of the body generates a vortex, which rolls up beside the body as the calculated velocity field for one cross-flow plane shows (Figure 21b.). This vortex can not be accounted for in the panel method. Figure 22. shows that in this case the velocities on the body surface are only influenced by the relatively weak down-wash of the wing. In the Euler result the vortex induced velocities are much greater and even cause the velocity vectors to change from a positive to a negative angle behind the wing.

Finally I would like to show the flow around a quite different configuration, and not at all a transonic case. It is the example of a VW principle car and it shows that the FBV version of our code can be widely used for a variety of flow problems. Figure 23. shows the car embedded in the whole grid system. The thicker lines match the block boundaries. The overall block number was 18 and even for this high block structure the ratio between I/O- and CPU-time could be kept below .3. Figure 24. shows the calculated isobars on the surface, while figure 25. shows the computed velocity field with a small vortex at the lower back part. At last figure 26 shows the convergence history of the averaged error and the drag coefficient.

Conclusion

The examples show that in some cases it is necessary to account for "real body" effects and to solve the Euler equations instead of the FPE to get the correct inviscid solution for transonic flows. Only the Euler methods are able to account for vorticies in the flow field, which may emerge from sharp corners. So the Euler methods, in their different block structured versions, are applicable to a wide range of flow problems and allow real 3-D calculations with a nearly unrestricted number of grid points within an acceptable amount of computing time. Even for cases with 18 blocks the rate between I/O- and CDU-time could be kept below .3 with an IBM 3083. For a CRAY 1 computer this rate lies at about .75. The comparisons of the different versions show that the convergence behaviour of all can be reduced drastically by using the well known multigrid technique, which for a blocked flow field could be further improved as mentioned above.

References

[1] Jameson, A., Caughey, D.A., "Finite Volume Method for Transonic Potential Flow Calculations." Proceedings, AIAA 3rd Computational Fluid Dynamics Conference, 1977

[2] Caughey, D.A., Jameson, A., "Recent Progress in Finite Volume Calculations for Wing-Fuselage Combinations." AIAA paper 79-1513, 1979

[3] Rizzi, A.W., Schmidt, W., "Study of Pitot-Type Supersonic Inlet-Flowfields Using the Finite Volume Approach." AIAA paper 78-1115, 1978

[4] Grashof, J., "Investigation of the Three-Dimensional Transonic Flow around an Air Intake by a Finite Volume Method for the Euler Equations." In: Transport Phenomena in Fluid Mechanics, Springer Verlag, Berlin/Heidelberg/ New York, 1982

[5] Middlecoff, J.F., Thomas, P.D., "Direct Control of the Grid Point Distribution in Meshes Generated Elliptic Equations." Proceedings, AIAA 4th Computational Fluid Dynamics Conference, 1979

[6] Yu, N.J., "Grid Generation and Transonic Flow Calculations for Wing-Body Configurations", Boeing Report D6-45277/1980, 1980

[7] Leicher, S., Fritz, W., Grashof, J., Longo, J., "Mesh Generation Strategies for CFD on Complex Configurations. Lecture Note in Physics, VOL. 170, pp. 329-334, Springer Verlag, 1982

[8] Lee, K.D., "3-D Transonic Flow Computations Using Grid Systems with Block Structure". AIAA paper 81-0998, 1981

[9] Hulst, T., "An Implicit Algorithm for Conservative Transonic Full Potential Equation using Arbitrary Mesh". AIAA Journal 17 1038-1045, 1979

[10] Baker, T.J., Forsey, C.R., "A Fast Algorithm for the Calculation of Transonic Flow Over Wing/Body Combinations". AIAA 5th Computational Fluid Dynamics Conference, p. 189-198

[11] South, J.C., Brandt, A., "The Multigrid Method: Fast Relaxation for Transonic Flows" 13th Annual Meeting of Society of Engineering Science, Hamptary VA, November 1976

[12] Jameson, A., "Acceleration of Transonic Potential Flow Calculations on Arbitrary Meshes by the Multiple Grid Method", AIAA 4th Computational Fluid Dynamics Conference, Williamsburg, VA, AIAA Paper 79-1458, July 1979

[13] Stock, H.W., "Integralverfahren zur Berechnung dreidimensionaler, laminarer und turbulenter Grenzschichten". Dornier FB 77/51 B, 1977

[14] Schmidt, W., Jameson, A., "Recent developments in finite volume time dependend techniques for two and three-dimensional transonic flows." VUI Lecture Series 1982-04, 1982

[15] Jameson, A., Baker, T.J., "Multigrid Solution of the Euler Equations for Aircraft Configurations". AIAA 22nd Aerospace Science Meeting, Reno, January 9-12, 1984

[16] Schmidt, W., Jameson, A., "Euler Solutions as limit of infinite Re-number for separated flows and flows with vortices. Lecture Note in Physics, Vol. 170, pp. 468-473, Springer Verlag, 1982

[17] Hummel, "On the vortex formation over a slender wing at large angles of incidence." AGARD-CP-247, High Angle of Attack Aerodynamics, 1978

[18] Hummel, "Untersuchungen über das Aufplatzen der Wirbel an schlanken Deltaflügeln." ZFW 13, Heft 5, 1965

[19] Hitzel, S.M., Schmidt, W., "Slender Wings with Leading-Edge Vortex Separation - A Challenger for Panel-Methods and Euler-Codes". AIAA 21st Aerospace Science Meeting, Reno, January 9-12, 1983.

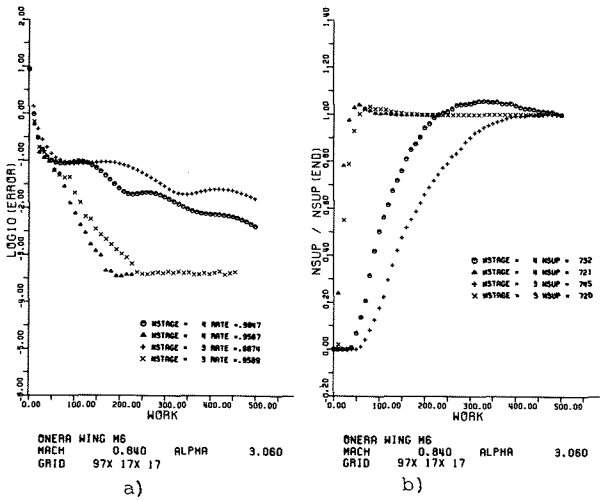

a) b)

Figure 1

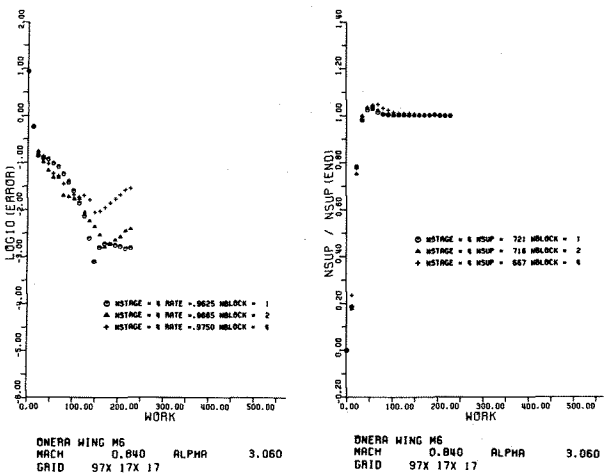

Figure 2 a)

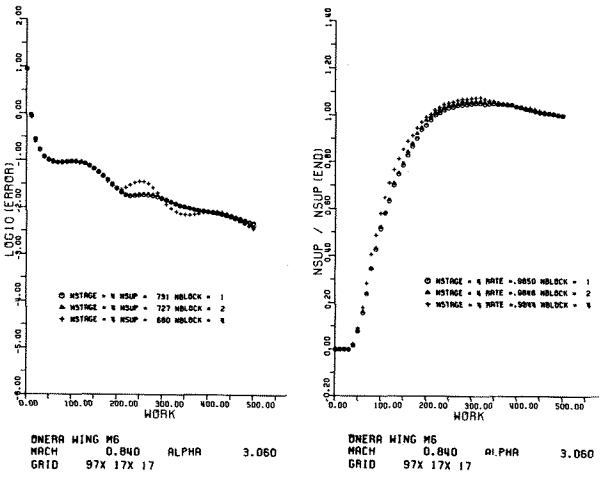

Figure 2 b)

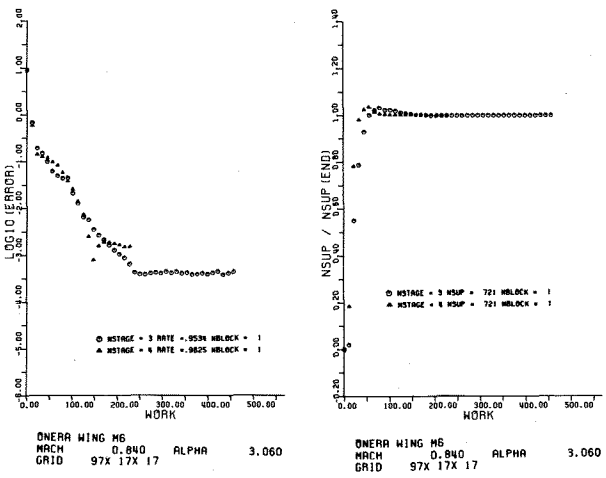

Figure 2 c)

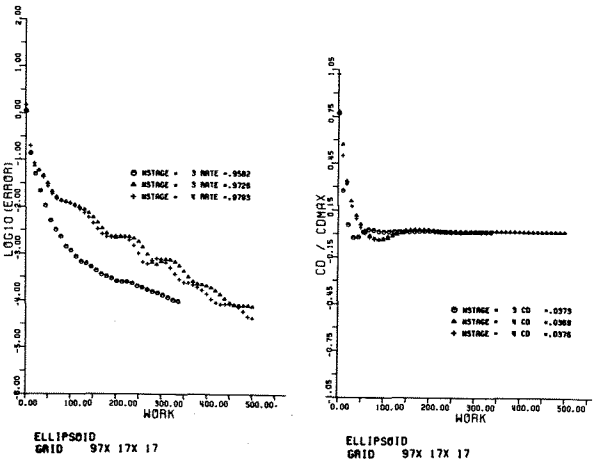

a) b)

Figure 3

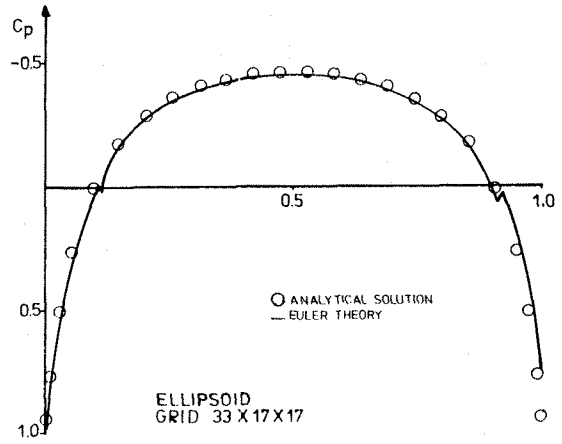

Figure 3 c)

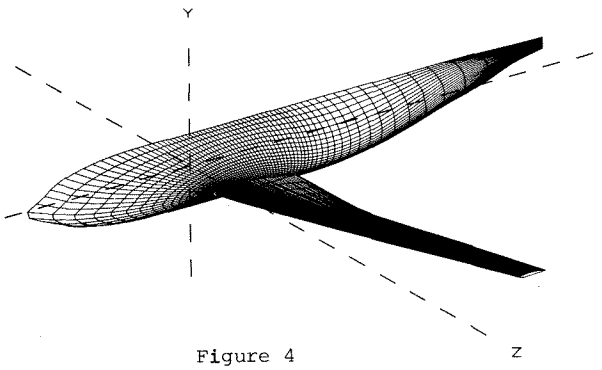

Figure 4

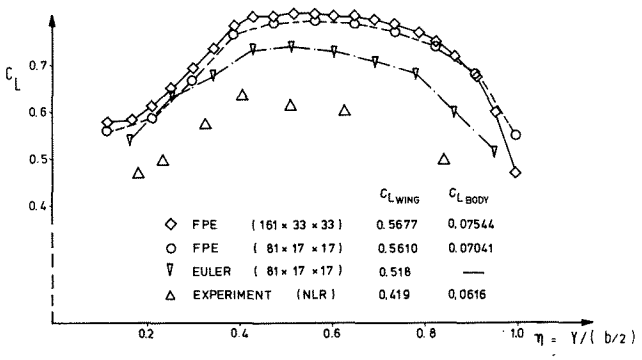

Figure 6

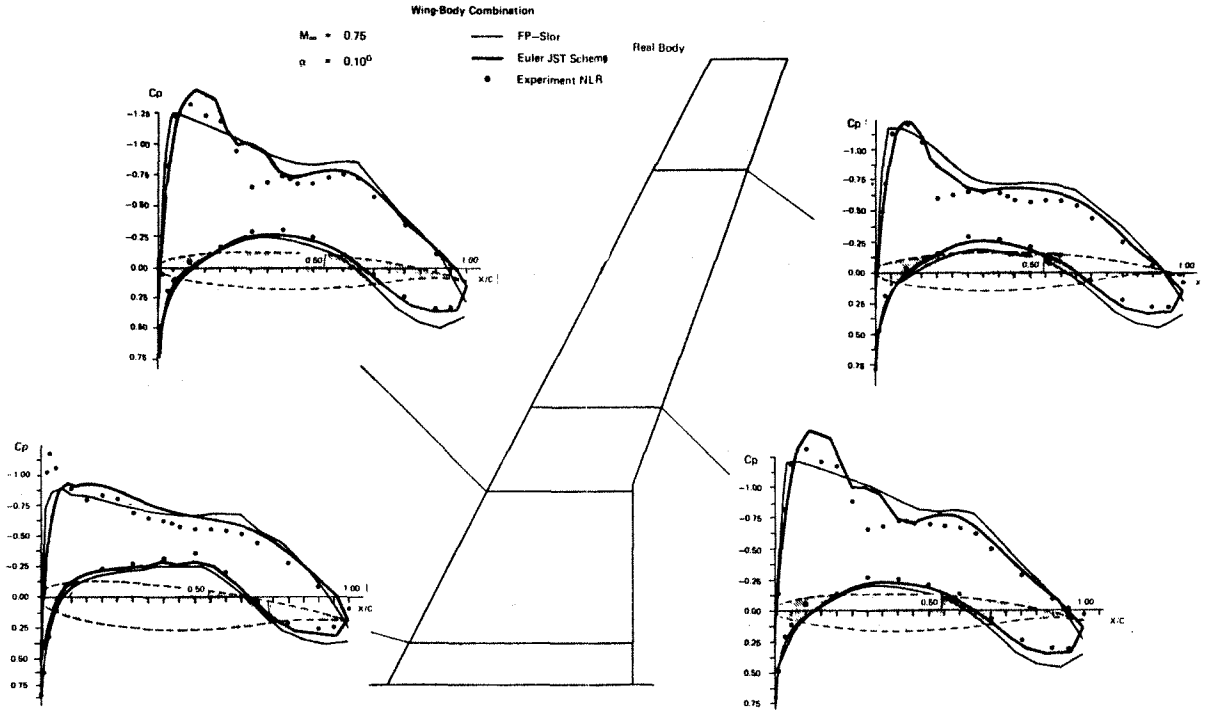

Figure 5

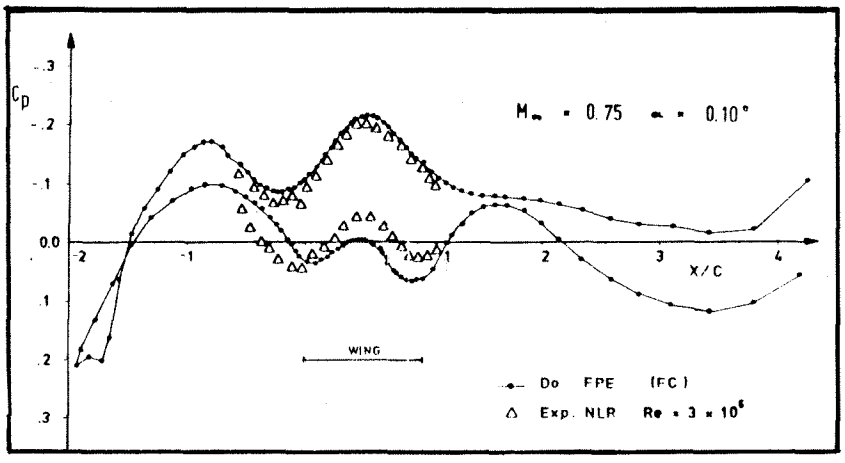

Figure 7

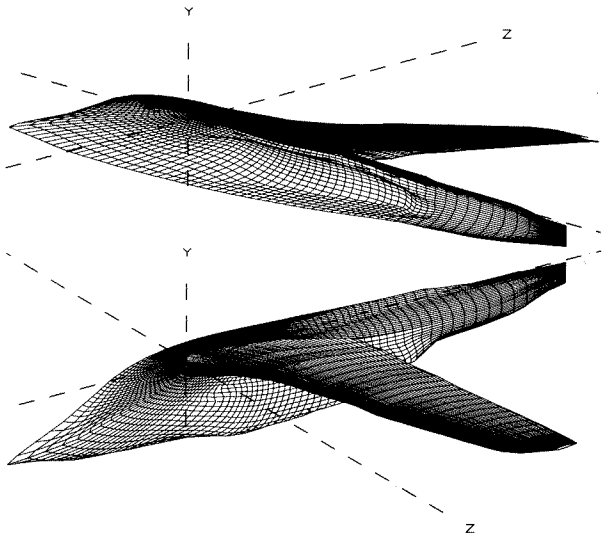

Figure 8

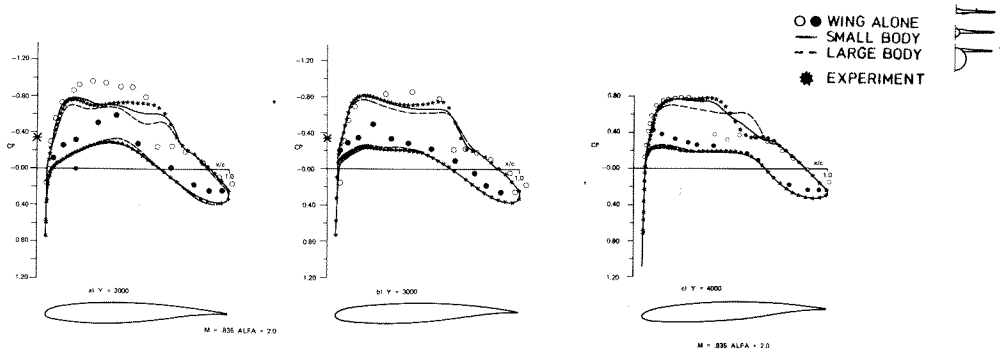

Figure 9 a)

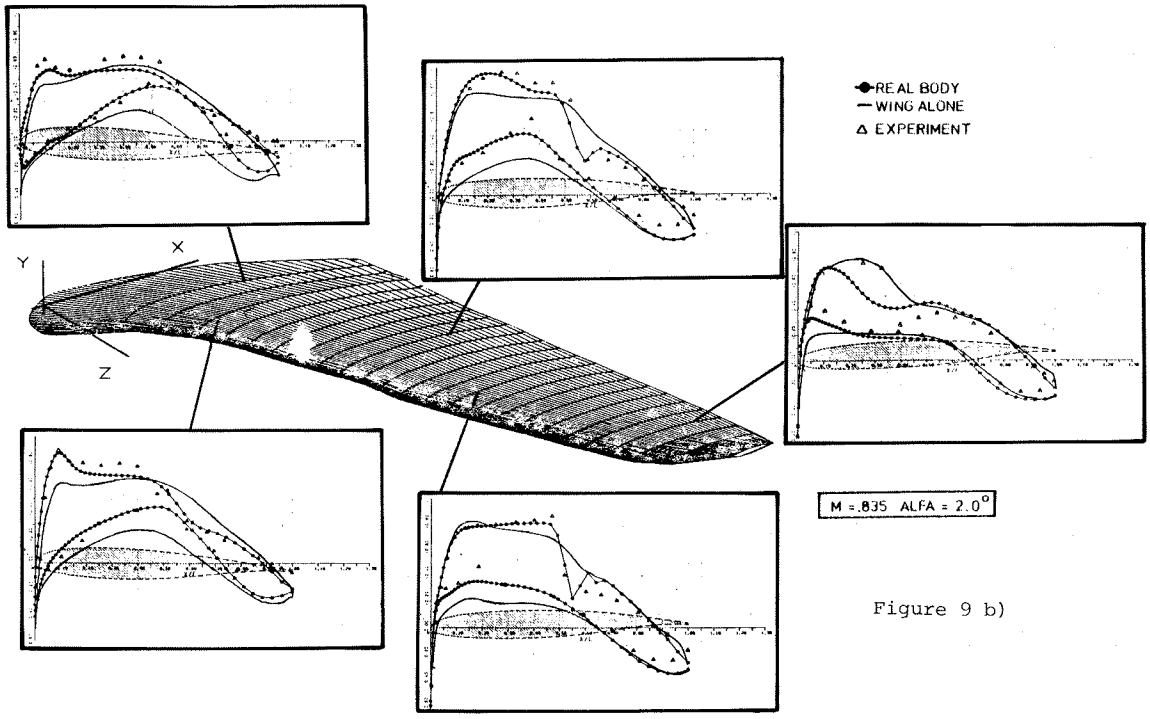

Figure 9 b)

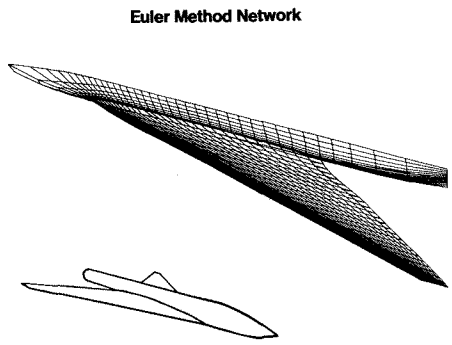

Figure 10

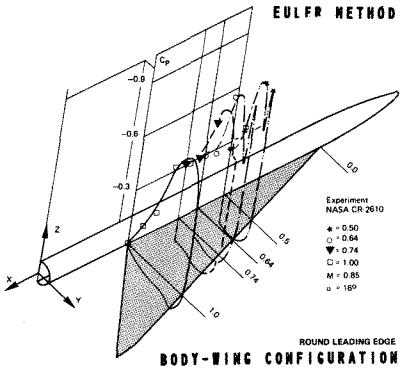

Figure 11

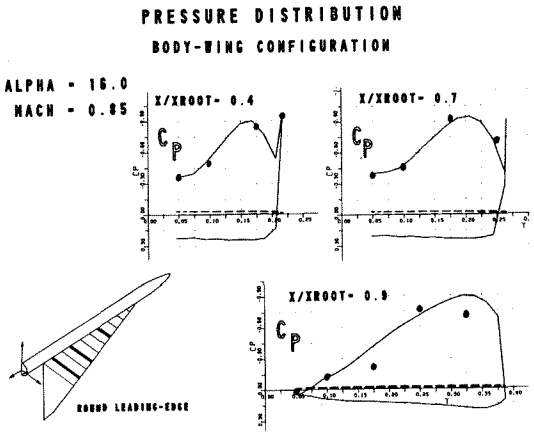

Figure 12

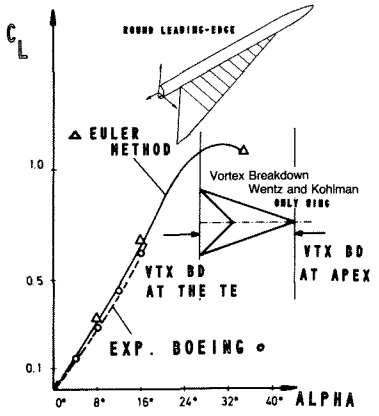

Figure 13

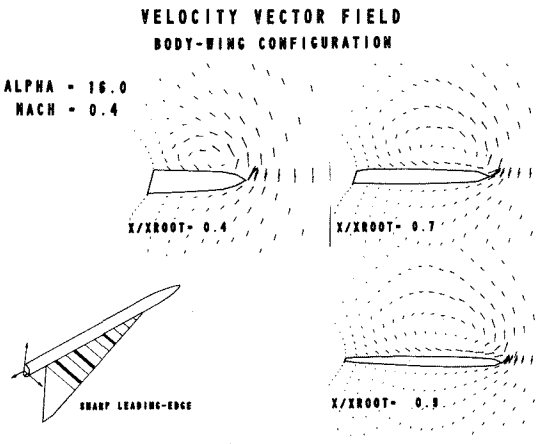

a)

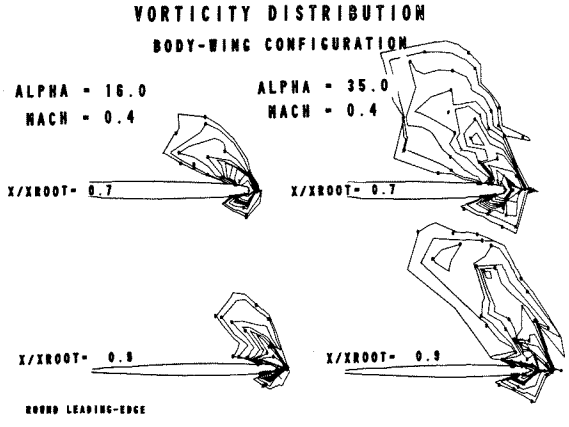

b)

Figure 14

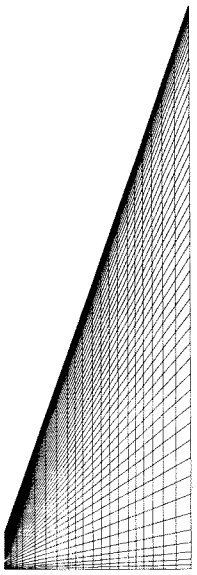

Figure 15

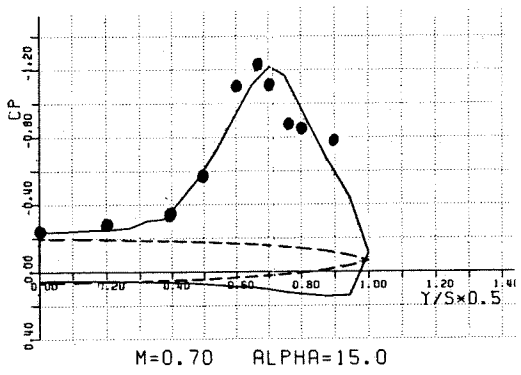

Figure 16

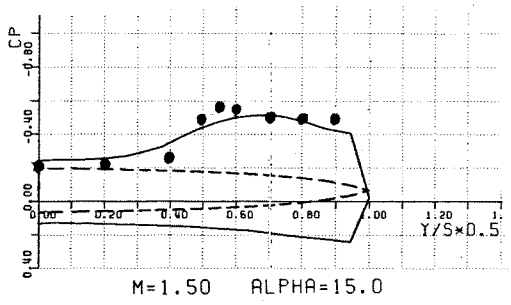

X/C=0.80

Figure 17

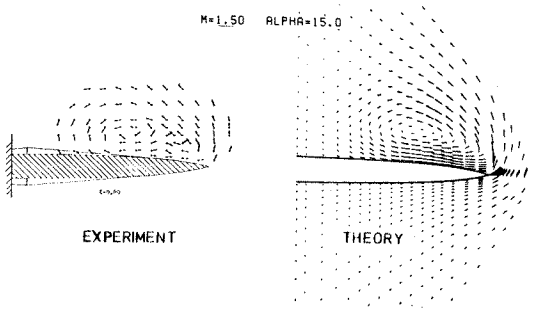

Figure 18

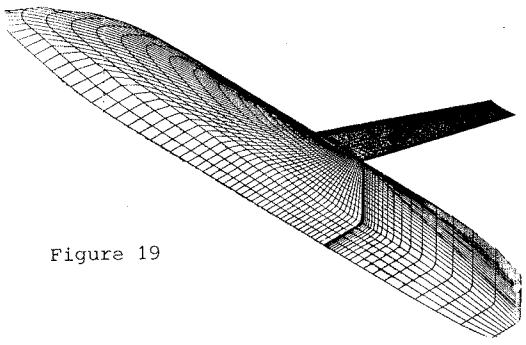

Figure 19

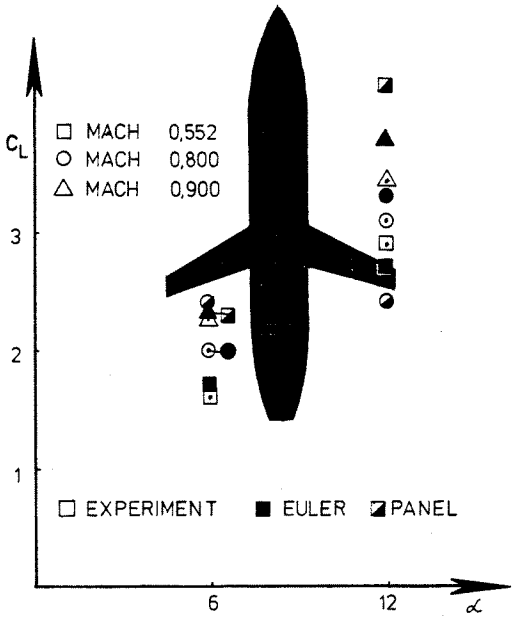

Figure 20

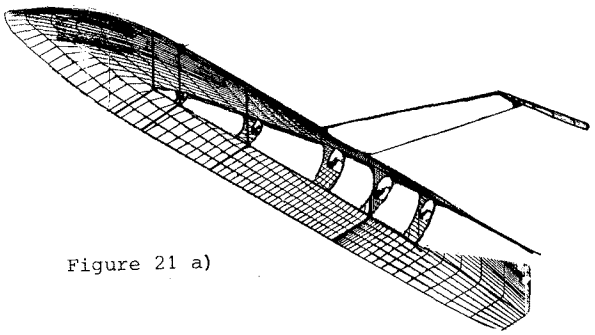

Figure 21 a)

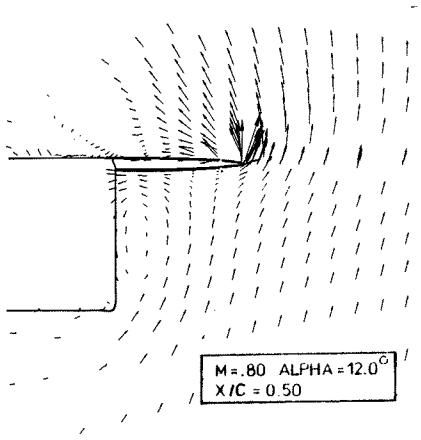

Figure 21 b)

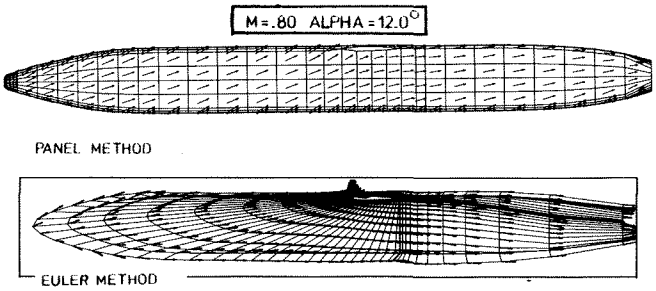

Figure 22

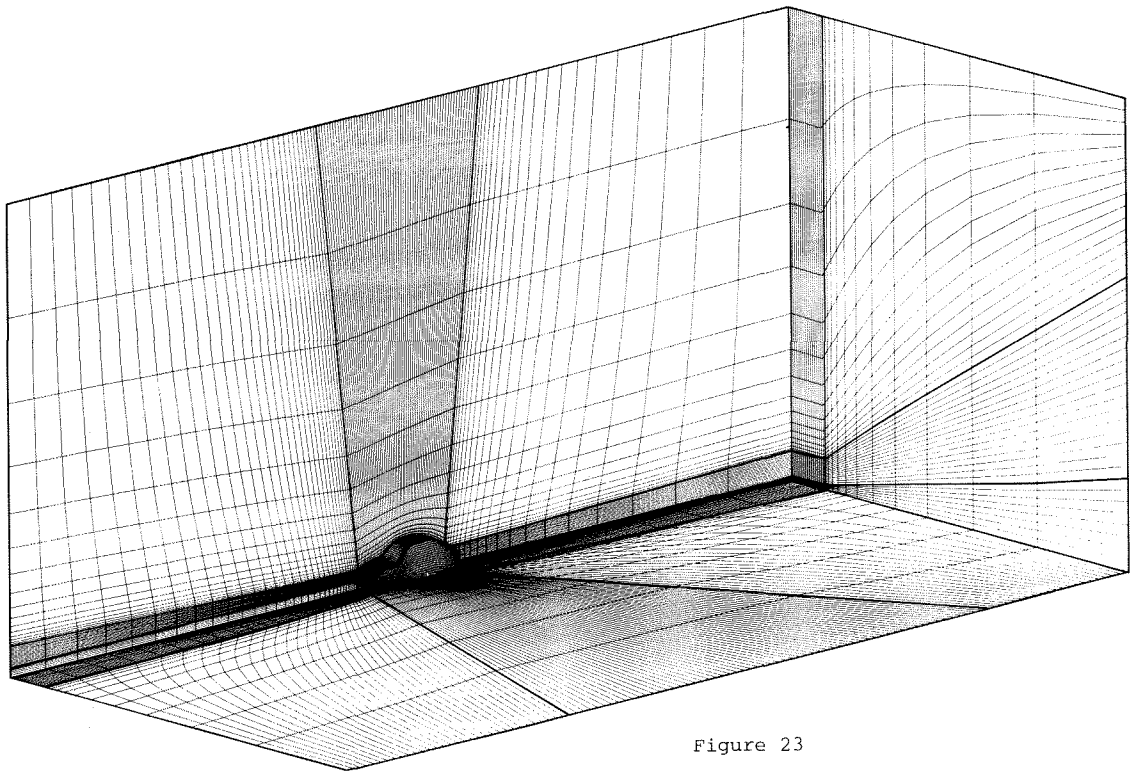

Figure 23

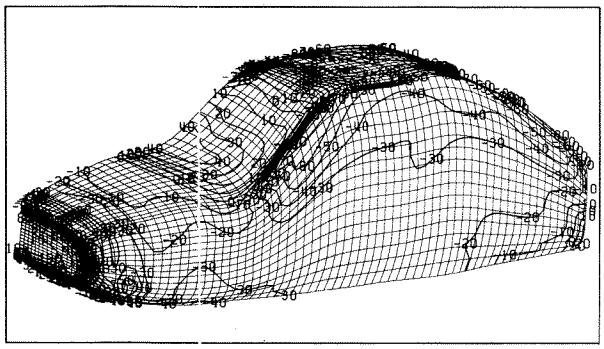

Figure 24

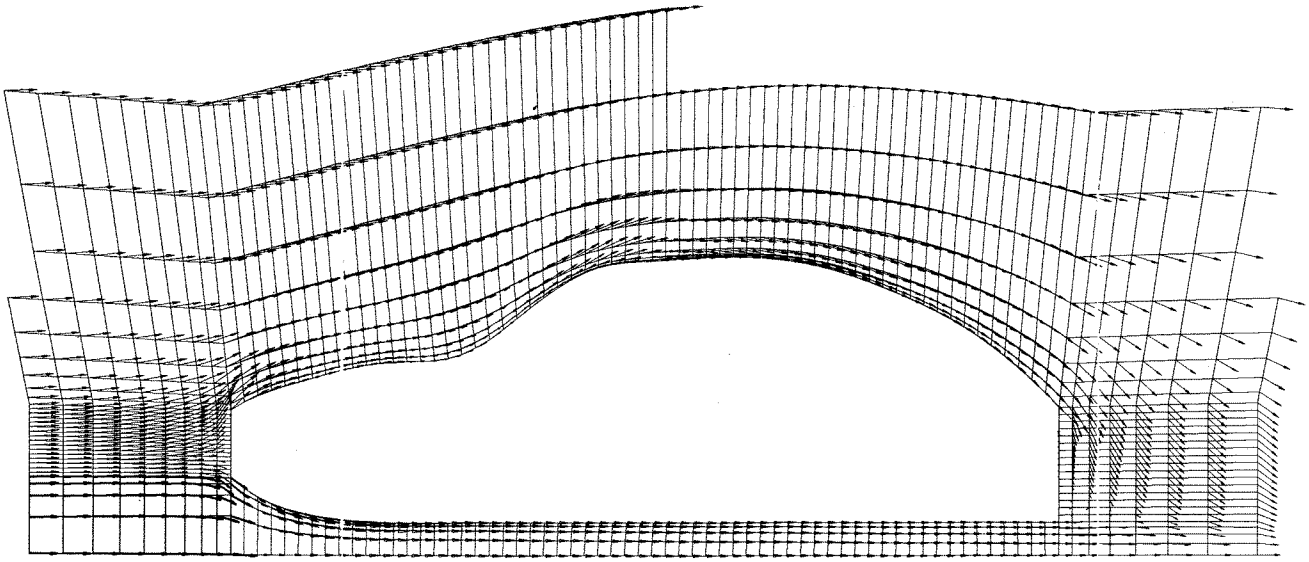

Figure 25

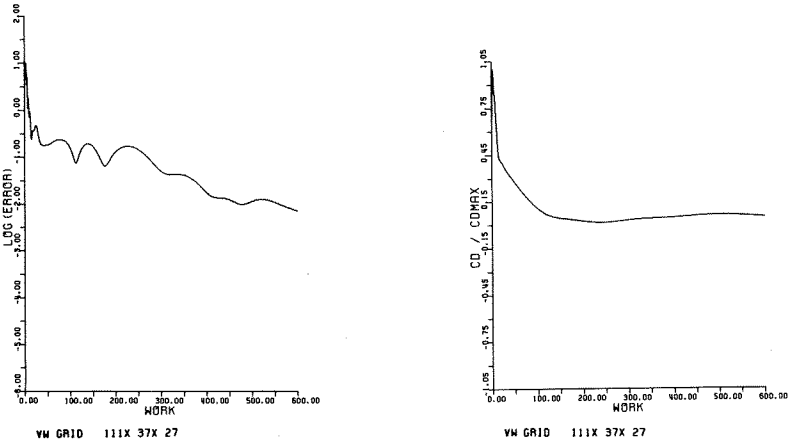

Figure 26